Catena 246 (2024) 108336

Contents lists available at ScienceDirect

Catena

journal homepage: www.elsevier.com/locate/catena

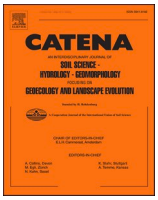

Investigating sediment sources using compound-specific stable isotopes and conventional fingerprinting methods in an agricultural loess catchment

Ghulam Abbas [a,*], Seifeddine Jomaa [a], Patrick Fink [a,b], Arlena Brosinsky [c,d], Karolina Malgorzata Nowak [e], Steffen Kümmel [e], Uwe-Karsten Schkade [f], Michael Rode [a,c]

[a] Department of Aquatic Ecosystem Analysis and Management, Helmholtz Centre for Environmental Research – UFZ, Magdeburg, Germany
[b] Department River Ecology, Helmholtz Centre for Environmental Research – UFZ, Magdeburg, Germany
[c] Institute of Environmental Science and Geography, University of Potsdam, Potsdam-Golm, Germany
[d] Remote Sensing and Geoinformatics Section, Helmholtz Centre Potsdam, GFZ German Research Centre for Geosciences, Potsdam, Germany
[e] Department Technical Biogeochemistry, Helmholtz Centre for Environmental Research – UFZ, Leipzig, Germany
[f] Division Radiation and Environment, Federal Office for Radiation Protection, D-10318 Berlin, Germany

ARTICLE INFO

Keywords:
Sediment fingerprinting
CSSI δ^{13}C-fatty acids
Crop-specific soil loss
C3 plants
C4 plants
Loess soils

ABSTRACT

Identifying crop-specific sediment sources is important, and conventional fingerprinting methods do not do so sufficiently, which limits their usefulness. The application of compound-specific stable isotopes (CSSIs) enables crop-specific sediment sources to be identified. To this end, this study applied the CSSI method to the intensively farmed loess soil Geesgraben catchment (75 km^2), in Central Germany. We used this catchment because the importance of different surface and subsurface sediment sources is unknown in temperate loess soil areas. The study also compared radionuclide and spectral fingerprinting methods, as well as spatiotemporal contribution of sediment sources. Specifically, the CSSI method, based on measuring δ^{13}C signatures of fatty acids, was applied to distinguish C3 and C4 plants, and riverbank sediment sources, which were identified using a multivariate mixing model. At the midstream site, the riverbanks contributed a mean of 12 % of the sediment, while the C3 and C4 plants each contributed 44 %. At the downstream site, according to the CSSI method, the riverbanks contributed 28 %, while the C3 and C4 plants contributed 9 % and 63 %, respectively. In comparison, according to the radionuclide and spectral methods, the downstream riverbanks contributed 41 % and 10 %, respectively; generally, this shows relatively lower contribution to the surface sediment contribution. The riverbanks contribution increased with catchment size, due to downstream changes caused by the deposition of surface sediments. Thus, results showed that CSSIs of δ^{13}C of fatty acids can distinguish C3 vs. C4 plants and surface vs. riverbank sources at the catchment scale. However, radionuclides remain useful in heterogeneous catchments because they are not influenced by soil type or lithology. This information is crucial for implementing agricultural practices that can decrease sediment loads to river ecosystems.

1. Introduction

Soil loss can decrease on-site soil fertility and agricultural yields, and lead to off-site degradation of river ecosystems and silting of dams. Sedimentation in a river can cause environmental problems (Walling, 1999). Human activities have impacted more than half of the Earth's surface, and the current rate of land use change, especially for agriculture, is unsustainable (Hooke et al., 2012). Many floodplains have experienced a wide range of sedimentation rates (Jeffries et al., 2003). Riverbanks as a sediment source have become the subject of increasing research interest in recent years (Abbas et al., 2023). Due to important processes in river dynamics (Wethered et al., 2015), riverbanks are an important and often underestimated source of sediment in the total load transported by water in catchments (Walling and Collins, 2005).

To date, most fingerprinting studies have used elemental geochemistry, radionuclides, mineral magnetism, and spectral properties. Because these fingerprinting methods have difficulty distinguishing crop- or plant-specific sources, there is much interest in using

* Corresponding author at: Department of Aquatic Ecosystem Analysis and Management, Helmholtz Centre for Environmental Research - UFZ, Magdeburg, Germany.
E-mail addresses: ghulam.abbas@ufz.de (G. Abbas), seifeddine.jomaa@ufz.de (S. Jomaa), patrick.fink@ufz.de (P. Fink), arlena.brosinsky@gfz-potsdam.de (A. Brosinsky), karolina.nowak@ufz.de (K.M. Nowak), steffen.kuemmel@ufz.de (S. Kümmel), uschkade@bfs.de (U. Schkade), michael.rode@ufz.de (M. Rode).

https://doi.org/10.1016/j.catena.2024.108336
Received 22 April 2024; Received in revised form 4 August 2024; Accepted 22 August 2024
Available online 7 September 2024

compound-specific stable isotope (CSSI) fingerprinting (Reiffarth et al., 2016). CSSIs of $\delta^{13}C$ of fatty acids (FAs) have been applied to distinguish the contributions of C4 plants (e.g., maize) from C3 plants (e.g., wheat) and other surface sources (Brandt et al., 2018a), as well as of specific land use types at the catchment scale (Blake et al., 2012; Brandt et al., 2016; Brandt et al., 2018a; Brandt et al., 2018b; Mabit et al., 2018). The ability of fingerprinting methods to distinguish sediment sources, such as surface vs. subsurface (radionuclides) or different crop types (CSSIs), can also be compared. The suitability of a given method may also depend on site conditions. If the results are not internally consistent, further investigation is required (Owens et al., 2016). For example, comparing $\delta^{13}C$-CSSIs of FAs, elemental geochemistry, and radionuclides (Hancock and Revill, 2013); elemental geochemistry and radionuclides (Rode et al., 2018); and $\delta^{13}C$-CSSIs of FAs and elemental geochemistry (Blake et al., 2012) often yields consistent results. To date, the use of the CSSI method to distinguish plant-specific sediment sources is often lacking at the catchment scale, especially in loess soils in Central Europe, and particularly in Germany. Additionally, to determine whether C3 and C4 plants, which have varying rates of upland erosion, also have different sediment contributions at the outlet to assess the implication of a simple modeling approach in future instead. Conventional fingerprinting methods can distinguish only surface sources based on land use types and cannot distinguish specific crop (C3 or C4 plants) sources.

Sediment fingerprinting uses a variety of properties (e.g., tracers), such as radionuclides (Gellis et al., 2017; Rode et al., 2018; Theuring et al., 2013), geochemical (Rode et al., 2018; Theuring et al., 2015), spectral (Brosinsky et al., 2014a; 2014b), environmental DNA (Evrard et al., 2019), mineral magnetic properties (Owens et al., 2000; Russell et al., 2001; Walling et al., 1999; Walling and Woodward, 1995), spectrocolorimetric visible-color-based parameters (Valente et al., 2020), and CSSIs (Blake et al., 2012; Brandt et al., 2018a; Gibbs, 2008; Hancock and Revill, 2013; Upadhayay et al., 2017; Upadhayay et al., 2018; Upadhayay et al., 2020). Other properties have been determined to be useful, but they can be applied only to contributions of sediment from specific land uses. The CSSI method is a new way to identify sediment sources from multiple land use types (Reiffarth et al., 2016). The $\delta^{13}C$-CSSIs of FAs have the potential to identify and trace crop-specific sediment sources at the catchment scale (Hancock and Revill, 2013). CSSIs of plant-derived FAs were successfully used to identify land use-specific sediment sources at the catchment scale (Gibbs, 2008; Upadhayay et al., 2017; Upadhayay et al., 2018). The soil from different crops is distinguished based on the FAs that adhere to the soil particles and act as labels for that particular sediment source (Gibbs, 2008; Upadhayay et al., 2017). The atmospheric CO_2-fixation pathways of plants yield different isotope-fraction patterns and thus different $\delta^{13}C$-FA values (Reiffarth et al., 2016). Other fingerprinting methods may be necessary to supplement the CSSI method for other surface and riverbank sources (Reiffarth et al., 2016). The ability of $\delta^{13}C$-CSSIs of FAs to distinguish riverbanks as a sediment source from areal upland sources is not commonly used. Information on CSSI contents of riverbanks is lacking especially in loess landscapes although riverbanks are considered an important sediment source at the catchment scale. Loess soils are the most fertile soils in Germany and are thus intensively used as arable land. Depending on specific climatic and topographical conditions, these soils are moderately to highly susceptible to soil erosion. The high fertility of these soils often results in a lack of riparian buffers, leaving riverbanks unprotected by higher vegetation. However, the resulting susceptibility to bank erosion is usually unknown. In addition, no comparative studies of fingerprinting methods in Germany exist. This knowledge gap hinders the availability of crucial information about how to select and apply tracers, which highlights the need for such studies. It is essential to understand the results of different fingerprinting methods to decide which tracers need to be applied in which context. In addition, studies of riverbank erosion and crop-specific soil losses have not been carried out in temperate loess areas, although these areas can lose large amounts of sediment (Cerdan et al., 2010). Thus, knowledge of sediment sources is necessary to decrease soil losses in these loess areas.

We hypothesized that $\delta^{13}C$-CSSIs of FAs can distinguish C3 and C4 plants and riverbank sediment sources at the catchment scale. The objectives of this study were to distinguish (1) crop-specific soil loss from C3 and C4 plants in loess soil catchment and (2) subsurface sources (e.g., riverbanks) and surface sources using CSSIs, including comparative assessment of the consistency, accuracy, and suitability of fingerprinting methods that used radionuclide tracers and spectral properties.

2. Materials and methods

2.1. Study site

The Geesgraben (area 75 km^2) (Fig. 1) is a small stream with a predominantly agricultural catchment (Table 1) that drains into the Bode River (catchment area 3200 km^2) near the Peseckendorf gauging station in Hadmersleben, Germany. The main land use of the catchment is non-irrigated arable land (77 %), followed by urban area (5.8 %). C3 plants, consisting of cereal crops such as winter wheat and winter barley, cover 79.5 % of the arable land, while C4 plants (maize) cover 20.5 % (Table S1). C4 plants cover decreases to 17.0 % in midstream subcatchment and to 5.7 % in the headwater subcatchment (Sauerbach), which is intensively used arable land. See Table S2 for details of the crop area. The Sauerbach subcatchment covers 1.35 km^2 and has 1.1 km of the stream that flows into an intensively instrumented gauging station of the Helmholtz Centre for Environmental Research – UFZ. The gauging station is equipped with an automated ISCO sampler and a multi-parameter probe. A multi-parameter water-quality probe (EXO^2, YSI Environment, USA) was deployed to simultaneously measure water temperature (precision: 0.001 °C, accuracy: ± 0.01 °C) and turbidity (precision: 0.01 FNU, accuracy: ± 2 % FNU). Discharge was measured every 10 min for the Sauerbach stream using a V-shaped weir and for the Geesgraben stream in Peseckendorf using a trapezoidal gauging station.

Soil erosion rates were estimated at a high spatial resolution using the Revised Universal Soil Loss Equation (RUSLE, based on Renard et al., 1996). All parameters were calculated individually for the Geesgraben catchment based on 19 land-cover classes (Preidl et al., 2020) and their cover and management (C) factor values (Schwertmann et al., 1987). The rainfall erosivity (R) factor was derived from contiguous radar-based rainfall data (Auerswald et al., 2019) and a soil erodibility map of the German Federal Institute for Geosciences and Natural Resources. The slope length and steepness (LS) factor was calculated using a high-resolution (30 m) Shuttle Radar Topography Mission (SRTM) Global data, and the support-practices (P) factor for the decrease in soil erosion was estimated from the type of farming. An upland erosion map was developed by multiplying all five factors together. Mean upland erosion rates were calculated by delineating boundaries of the Geesgraben, midstream, and Sauerbach catchments by processing Shuttle Radar Topography Mission data in ArcMap software (Table 1). Arc Hydro Tools of ArcMap were used to delineate catchments to create shapefiles that were then used to estimate soil erosion rates using geoprocessing tools of ArcMap.

2.2. Sediment sources and sediment sampling

Before field sampling campaigns, field surveys were performed and satellite images from Google Earth were examined. The surveys were used to collect information about the connectivity of potential sampling sites in the river network. The potential sediment sources were selected based on soil erosion (1) from surface sources (non-irrigated arable land) and (2) subsurface sources (riverbanks).

The sampling sites were selected based on their erodibility, accessibility, and connectivity to the river network. After this survey, turbidity sensors were installed for two years (2020–2021) at the gauging station of the Geesgraben outlet and nested subcatchments (i.e., midstream and

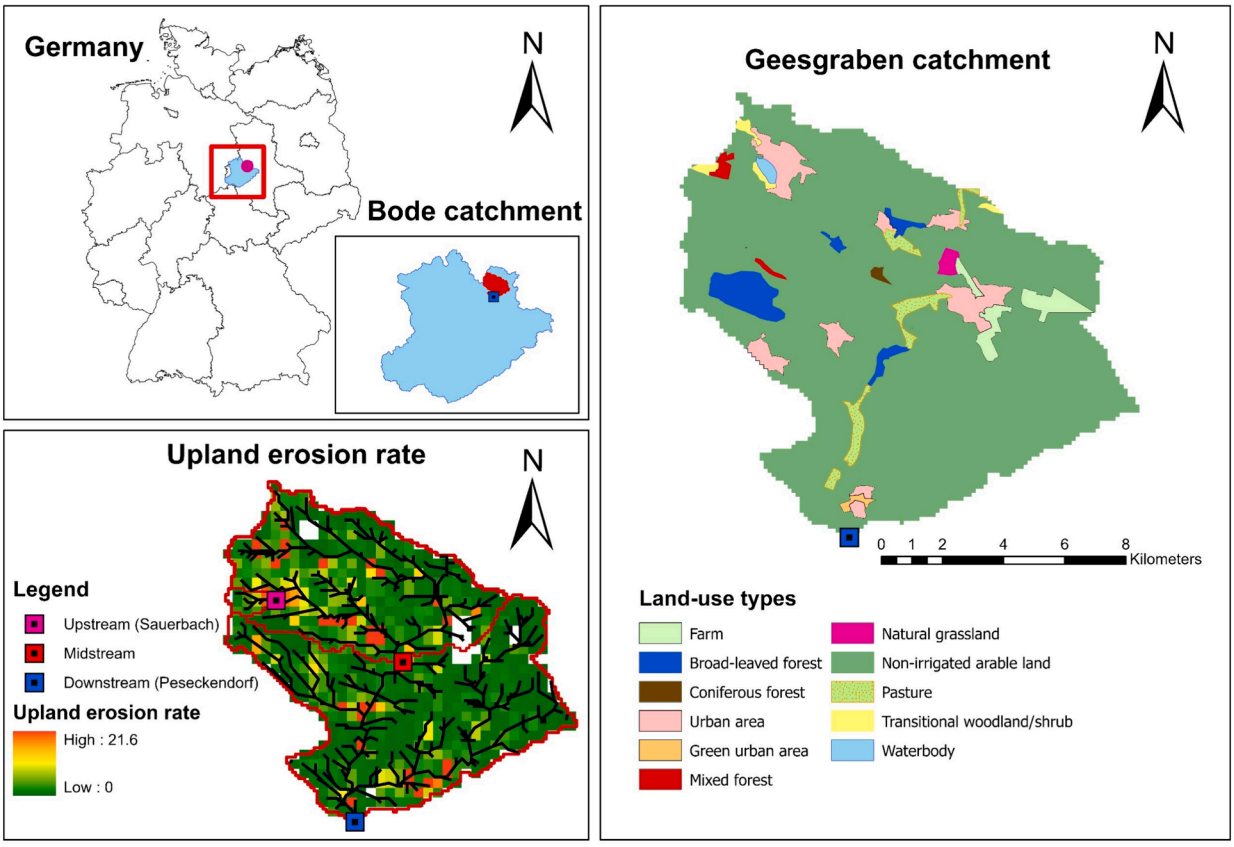

Fig. 1. Characteristics of the Geesgraben catchment (land use map) and upland erosion rate (t ha^{-1} yr^{-1}).

Table 1
Summary of RUSLE-based calculated mean upland erosion rates (t ha^{-1} yr^{-1}) with reference year 2020 for the Geesgraben at its three nested catchments (downstream outlet at Peseckendorf, midstream, and upstream at Sauerbach).

Catchment characteristics	Geesgraben at Peseckendorf	Geesgraben midstream	Sauerbach (headwater)
Area (km^2)	75	32.1	1.35
Arable land use (km^2)	58	22.5	1.05
Arable erosion rate	0.84	0.96	0.75
C3 plants erosion rate	0.63	0.80	0.78
C4 plants erosion rate	1.58	1.65	0.48

Sauerbach) to measure turbidity in order to calculate sediment loads at multiple catchment scales. The soil and sediment sampling depended on the sediment source types selected (i.e. arable C3 and C4 plants and riverbanks). Potential sediment sources were classified by soil type, land use, and upland erosion rate. The soil surface (arable land) was sampled using a stratified sampling design based on major soil and land use types and the upland erosion rate. All soil types and the main land use (arable land) were used to create stratified sampling units by superimposing the soil, land use, and upland erosion maps. Each composite soil sample of C3 and C4 plants consisted of 10 subsamples from 10 locations within 40 m^2. All soil samples were taken from the top 1–2 cm of the soil. Soil samples from the riverbanks were collected by scraping soil from the full vertical extent of observed and actively eroding profiles, with each composite sample weighing at least 1 kg and being packed into plastic bags (Fig. 2).

Suspended-sediment samples were collected from fresh suspended-sediment deposits near the gauging stations, especially after runoff events. Sampling campaigns 1, 2, and 3 were conducted in June and November 2020, and May 2021 respectively (Table 2). The source samples (arable land and riverbank) from all campaigns were pooled together in the mixing model and sediment contribution from each campaign was estimated regarding sediment sample from that specific campaign. The soil and sediment samples were collected from the field and transported to the sediment laboratory at the Helmholtz Centre for Environmental Research-UFZ, Magdeburg, Germany, for further preparation before analysing fingerprinting properties.

2.3. Laboratory analysis

Soil and sediment samples were oven-dried at 60 °C, ground, and then mechanically sieved to < 63 μm. The number of soil and sediment samples needed for laboratory analysis was collected and packed into plastic containers.

2.3.1. Extraction, fractionation, and derivation of fatty acids

Extraction of FAs included the extraction itself, separation of lipid groups, derivation, and preparation for gas chromatography (GC), as described by Nowak et al. (2011). In the first step, 10 g of each soil and sediment sample were placed into a screw-cap vial, to which a mixture of phosphate buffer (0.05 M, 20 ml), methanol (50 ml), and chloroform (25 ml) was added. The samples were then mechanically shaken for 2 h. After shaking, 25 ml each of H_2O and $CHCl_3$ were added, and the vials

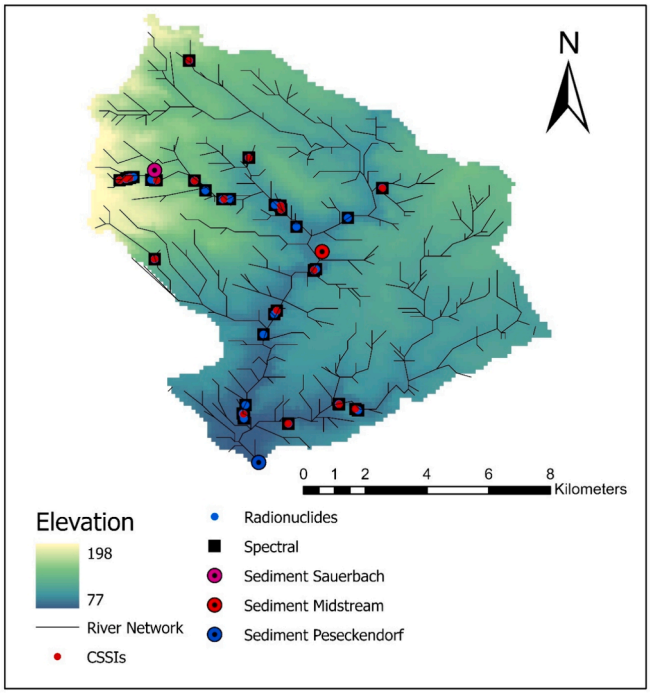

Fig. 2. Sampling sites distribution for Geesgraben catchment.

Table 2
Number of soil and sediment samples collected for each of the three fingerprinting methods during campaigns 1 (June 2020), 2 (November 2020), and 3 (May 2021) number in brackets shows sediment samples.

Fingerprinting method	Campaign 1	Campaign 2	Campaign 3
Compound-specific stable isotopes	18 (3)	–	–
Radionuclides	12 (3)	17 (3)	22 (3)
Spectral	18 (3)	22 (3)	22 (3)

were left overnight to separate the phases completely. The next day, the upper aqueous phase was discarded using a Pasteur pipette as a separation funnel. The $CHCl_3$ phase was collected, dried using solid-phase-extraction columns with ca. 1 cm of Na_2SO_4, and transferred to a new screw-cap vial. The soil was then rinsed again with a small additional amount of $CHCl_3$. The $CHCl_3$ phase was processed as before and combined with the first portion. Finally, the solvent was evaporated under a gentle stream of N_2 gas, and the residue was dissolved in 1 ml $CHCl_3$.

In the second step, lipid groups were separated. Silica gel columns were prepared by suspending 2.5 g silica gel (UniSil®) in 25 ml 0.02 M ammonium acetate in methanol. This suspension was transferred to solid-phase-extraction columns using a Pasteur pipette. The silica gel was washed with 25 ml each of acetone and $CHCl_3$. The sample prepared during the first extraction step was added and eluted with one volume (25 ml/2.5 g silica gel) of $CHCl_3$ for neutral lipids and one volume of acetone for glycolipids. Finally, phospholipids were eluted by adding three volumes (75 ml/2.5 g silica gel) of methanol. The phospholipid fraction was collected separately for each sample in screw-cap vials, and the solvent was evaporated under a gentle N_2 gas flux. After evaporation, the dry phospholipid samples were derived to FA methyl esters (FAMEs) in a mixture of 2250 µl methanol and 250 µl trimethylchlorosilane at 60 °C for 2 h. Afterward, samples were evaporated under a gentle stream of N_2 gas. Finally, 50 µl of icosanoic acid (C20:0) dissolved previously in hexane was added as an internal standard to each dried sample and analysed via gas chromatography-mass spectrometry (GC–MS) and gas chromatography-isotope ratio mass spectrometry (GC-IRMS), respectively.

FAMEs were separated using GC–MS (HP 6890, Agilent) equipped with a BPX-5 column (Trajan, 30 m × 0.25 mm × 0.25 µm film), and the following temperature program: initial temperature 50 °C (hold for 1 min), heat to 250 °C (0 min) at 4 °C/min and finally to 300 °C (10 min) at 2 °C/min. The injector was set at 280 °C, and the helium flow was 2.5 mL/min. FAMEs were identified by comparing the retention times and mass spectra to those of a standard mixture of Bacterial Acid Methyl Esters (Sigma Aldrich).

Carbon isotope signatures ($\delta^{13}C$) were analysed using an IRMS (MAT 253, Thermo Scientific) interfaced with a GC system (7890 A, Agilent) via a GC-IsoLink and a ConFlo IV interface (Thermo Scientific). The combustion reactor was maintained at 1000 °C. Samples were separated in a BPX-5 column (Trajan, 50 m x 0.32 mm x 0.5 µm film) using a helium carrier gas flow of 2 mL/min and the following temperature program: initial temperature 70 °C (1 min), heat to 130 °C (0 min) at 20 °C/min, to 150 °C (5 min) at 2 °C/min, to 165 °C (5 min) at 2 °C/min, to 230 °C (0 min) at 2 °C/min, and finally to 300 °C (5 min) at 20 °C/min. The injector temperature was kept at 250 °C, and a split ratio of 1:5 or 1:3 was used depending on the concentration of the sample. Each sample was analysed in triplicate. The total uncertainty in $\delta^{13}C$ measurements (i.e., accuracy plus reproducibility) was ± 0.5 ‰.

2.3.2. *Spectral fingerprinting*

Spectral reflectance data was collected using a high-resolution portable spectroradiometer (FieldSpec3, ASD). The laboratory setup included (1) a black box with two halogen lamps at 45° zenith viewing angle and (2) the spectroradiometer with 8° fore-optic, viewing nadir at 7 cm from the sample surface. The soil and sediment samples were placed in shallow plastic containers 4.5 cm in diameter. Before measuring samples, a white reference was placed on the turntable black box, and the spectroradiometer was optimized. The spectroradiometer was then calibrated with the white reference to serve as a 100 % reflectance baseline for all subsequent measurements. Finally, the samples were measured in relative reflectance and rotated 90° after each measurement. Although conditions were stable, the calibration was repeated after every five samples. The repeated measurements per sample were averaged, minor detector jumps were corrected, and spectra were smoothed using a Savitzky-Golay filter. From these smoothed-spectra, RGB values were calculated by averaging wavelength intervals that corresponded to Landsat RGB bands. From these RGB values, 21 color-based parameters were calculated using ColoSol software (Viscarra Rossel et al., 2006), and 77 physically based spectral features were calculated. A comprehensive understanding of spectral properties can be found in original sources (Bayer et al., 2012; Chabrillat et al., 2011).

2.3.3. *Radionuclide fingerprinting*

Radionuclide activity in the sediment samples was measured for ^{7}Be, $^{210}Pb_{ex}$, and ^{137}Cs using gamma spectroscopy at the German Federal Office of Radiation Protection. Aluminum bottles (205 ml at 8 cm fill height) were used to analyse bulk samples in coaxial high-purity germanium detectors. The gamma spectra were analysed using Genie 2000 software (Canberra Industries, Inc., Meriden, Connecticut, USA). Counting times of 25,000–80,000 s were used to measure the activity of ^{7}Be, ^{137}Cs, and $^{210}Pb_{ex}$ (250 ml aluminum bottles) to detect minimum levels of 0.5 Bq kg^{-1} for ^{137}Cs and 5 Bq kg^{-1} for ^{7}Be. These thresholds also ensured reliable detection of $^{210}Pb_{ex}$, which was calculated by subtracting the supported activity from the total ^{210}Pb activity (measured at 46.5 keV) using two ^{226}Ra daughters (i.e., ^{214}Pb and ^{214}Bi) (Rode et al., 2018). Other radionuclides such as ^{40}K, ^{228}Ra, ^{228}Th, ^{238}U, and ^{226}Ra were also detected from the soil and sediment samples but were not used in the sources estimation.

2.4. Correction factors

A correction factor (Z) was included in the linear multivariate mixing model used to distinguish sediment sources because particle size strongly influences the concentration of fingerprinting properties. If a correction factor is not used, concentrations of materials with different particle-size characteristics cannot be compared (Collins et al., 1997b). Soil and sediment samples must have the same particle-size distribution to determine the δ^{13}C-FAs (Upadhayay et al., 2020). Specific surface area was used to calculate Z because it strongly influences the concentration of fingerprinting properties. Particle-size distribution was determined using a laser-diffraction particle-size analyzer (LA-950, Retsch) that measured particles 100 nm to 2 mm in size. It uses laser scattering and an autosampler that automates the analysis. The preparation included removing the organic and carbonate fractions from the soil samples before measuring particle-size distribution. Z was calculated as the specific surface area of the individual suspended sediment divided by the mean specific surface area of each source type (Table 3).

2.5. Sediment-load measurements using turbidity sensors

Suspended-sediment concentration was calculated from turbidity measurements and their correlation with suspended sediments. Turbidity sensors were first tested in the laboratory by creating specific sediment concentrations and then developing regressions between them and turbidity. After the sensors were calibrated in the laboratory, they were installed at three locations: upstream (Sauerbach gauging station), midstream, and downstream (Peseckendorf gauging station). A multi-parameter logger was also installed at the Sauerbach gauging station with additional measurements of turbidity and discharge. Discharge was measured at the Peseckendorf gauging station of the State Office for Flood Protection and Water Management of Saxony-Anhalt by measuring the water level. The turbidity recorded by these two sensors was compared. The sensors were cleaned by an automatic wiper every 6 h, and turbidity was measured every 10 min. Discharge was also measured every 10 min at the gauging stations. The sites were visited monthly to ensure that the sensors were working properly and that their batteries still had power, and to collect data from sensor memory cards.

2.6. Statistical techniques for fingerprinting discrimination

Before using the mixing model, the fingerprinting method's conservativeness and power to distinguish sediment sources at all sites needed to be tested. Several statistical techniques were used to select the final set of properties for the mixing model. Before assessing the discrimination power of the properties, the properties were screened using a two-step procedure: (1) selecting properties that had an F-ratio (i.e. ratio of between-group to within-group variance) greater than 1.5 and then (2) using a range test to select properties whose concentration in the sediment lay between those of the sources. Properties outside of this range were excluded from further analysis. After the range test, a Kruskal-Wallis test was applied to compare the ability of the fingerprinting properties to distinguish the sediment sources (C3 and C4 plants) and riverbanks. The properties were tested using discriminant function analysis (DFA) before using the linear multivariate mixing model to identify sediment sources. The DFA showed which fingerprinting tracers or final set of properties distinguished the sediment sources the best. The biplots were created to analyse the results. The soil and sediment samples must plot along the same lines or in the same space in biplots to show conservative behavior of fingerprinting properties.

2.7. Mixing model and goodness-of-fit

The relative contribution of sediment sources was estimated using the linear multivariate mixing model based on the specific land use types and riverbanks, as well as surface and subsurface sources (Lizaga et al., 2020):

$$\sum_{j=1}^{m} a_{i,j}.\omega_j = b_i$$

where $\alpha_{i,j}$ is fingerprinting property i $(i = 1 \text{ to } n)$ of source type j, b_i is fingerprinting property i of the sediment, ω_j is the unknown relative contribution of source type j $(j = 1 \text{ to } m)$, n is the total number fingerprinting properties used, and m is the number of sediment sources selected. The equation must satisfy two conditions (1) the sediment

Table 3
Correction factors for soil samples from C3 and C4 plants, arable land, and riverbanks.

Correction factor	Campaign	C3 plants	C4 plants	Arable land	Riverbanks
Midstream	1	0.93	0.94	0.93	0.89
Downstream	1	1.19	1.15	1.17	1.16
Downstream	2	–	–	1.01	1.12
Downstream	3	–	–	0.86	0.97

Table 4
Tracers tested using the F-ratio, range test, and Kruskal-Wallis test and those ultimately selected (asterisks, $P < 0.05$) to identify the contribution of surface and riverbank sources at the midstream site.

Tracer	F-ratio	Within range	H statistic	P value
Tetradecanoic acid (C14:0)	3.32	no	–	–
Cis-9-hexadecanoic acid (C16:1ω7)	25.4	no	–	–
Hexadecanoic acid (C16:0)	2.29	no	–	–
Anteiso-heptadecanoic acid (a-17:0)	1.74	no	–	–
Cis-9,10-methylene hexadecanoic acid (cy17:0)	2.22	yes	2.87	0.238
Octadeca-x,x-dienoic acid (C18:2)	3.05	no	–	–
Octadeca-6,9-dienoic acid (C18:2ω6,9)	2.42	no	–	–
Octadecanoic acid (C18:0)	4.66	no	–	–
10-methyl octadecanoic acid (10me18:0)	1.79	no	–	–
Eicosenoic acid (C20:1)	7.27	yes	6.07	< 0.05*
Docosanoic acid (C22:0)	2.54	no	–	–
Tricosanoic acid (C23:0)	6.48	yes	7.89	< 0.05*
Pentacosanoic acid (C25:0)	4.05	no	–	–
Hexacosanoic acid (C26:0)	2.72	no	–	–
Heptacosanoic acid (C27:0)	2.34	no	–	–
Nonacosanoic acid (C29:0)	3.62	yes	5.97	0.050

Table 5
Tracers tested using the F-ratio, range test, and Kruskal-Wallis test and those ultimately selected (asterisks, P < 0.05) to identify the contribution of surface and riverbank sources at the downstream site.

Tracer	F-ratio	Within range	H statistic	P value
Tetradecanoic acid (C14:0)	2.32	no	–	–
Anteiso-pentadecanoic acid (a-15:0)	3.32	yes	7.38	< 0.05*
Iso-hexadecanoic acid (i-16:0)	4.46	yes	8.09	< 0.05*
Cis-9-hexadecanoic acid (C16:1ω7)	9.97	yes	11.1	< 0.05*
Hexadec-5-enoic acid (C16:1ω5)	3.71	no	–	–
Hexadecanoic acid (C16:0)	5.35	no	–	–
Anteiso-heptadecanoic acid (a-17:0)	2.26	yes	3.40	0.183
Octadeca-6,9-dienoic acid (C18:2ω6,9)	3.45	yes	5.88	0.053
Cis-11-octadecanoic acid (C18:1ω7)	15.5	yes	11.5	< 0.05*
Octadecanoic acid (C18:0)	2.12	yes	4.09	0.130
10-methyl octadecanoic acid (10me18:0)	2.88	no	–	–
cis-9,10-Methylene octadecanoic acid (cy19:0)	2.54	yes	3.32	0.190
5,8,11,14-tetraenoic acid (C20:4)	8.82	yes	9.16	< 0.05*
Eicosenoic acid (C20:1)	7.05	yes	8.73	< 0.05*
Docosanoic acid (C22:0)	2.47	yes	3.19	0.203
Tricosanoic acid (C23:0)	6.03	no	–	–
Tetracosanoic acid (C24:0)	2.07	yes	6.02	< 0.05*
Pentacosanoic acid (C25:0)	7.47	no	–	–
Heptacosanoic acid (C27:0)	3.27	yes	4.25	0.119
Nonacosanoic acid (C29:0)	1.56	yes	2.69	0.261

Table 6
Tracers selected using discriminant function analysis to identify the contribution of surface and riverbank sources. Asterisks identify significant (level < 0.1) tracers.

Site	Tracer	Wilks lambda	F statistic	level
Midstream	Eicosenoic acid (C20:1)	0.35	7.27	< 0.1*
	Tricosanoic acid (C23:0)	0.38	6.48	< 0.1*
Downstream	Cis-11-octadecanoic acid (C18:1ω7)	0.33	15.5	< 0.1*
	Eicosenoic acid (C20:1)	0.22	7.78	< 0.1*

contribution from the sources must have a value between 0 and 1, and (2) the sum of all the contributions must equal 1.

The goodness-of-fit (GOF) of the model was calculated from the sum of squares of the relative error:

$$\mathrm{GOF} = 1 - \frac{1}{n} \times \left(\sum_{i=1}^{n} \frac{\left| b_i - \sum_{j=1}^{m} \omega_j a_{ij} \right|}{\Delta_i} \right)$$

where Δ_i is the range of fingerprinting property i, calculated as a normalized factor. The multivariate mixing model was run for 3000 model iterations; for each iteration, the goodness-of-fit was calculated as the sum of squares of the relative error. The model was configured to select the 10 best results with the highest GOF obtained from 3000 iterations.

3. Results

3.1. Identification of specific crop-type sources based on CSSI tracers

3.1.1. Statistical discrimination power

At the midstream site, the final set of CSSI tracers selected showed concentrations of δ^{13}C-FAs in the sediment samples that lay between those soils of C3 and C4 plants and the riverbanks. The tracers were selected using the Kruskal-Wallis test (P < 0.05) at the midstream (Table 4) and downstream sites (Table 5). Afterward, the final set of tracers was selected using DFA (level < 0.1) including two tracers (C20:1 and C23:0) at the midstream and two tracers (C18:1ω7 and C20:1) at the downstream sites (Table 6), which were used to identify sediment sources in the mixing model. See Table S3 for the δ^{13}C-CSSIs of FAs, number of samples, mean, and coefficient of variation for the three sediment sources.

The biplot of selected δ^{13}C-CSSIs of FAs (Fig. 3) showed further evidence of the conservative behavior of the tracers. This was consistent with the selected FA properties of the soil and sediment samples at the midstream and downstream sites. The soil and sediment samples were more scattered for C20:1 and C23:0 midstream than for C20:1 and C18:1ω7 downstream because the midstream site had a smaller sample size. The riverbank samples were also more scattered than the surface samples.

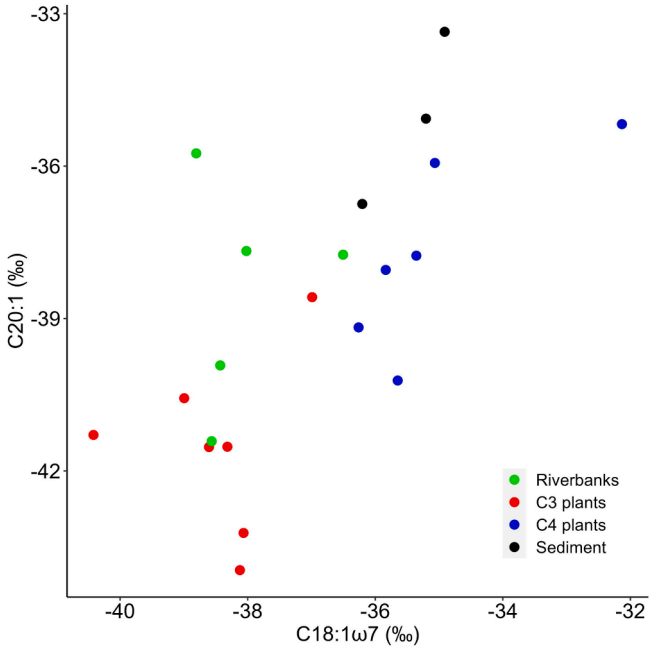

Fig. 3. Biplot of δ^{13}C-Compound Specific Stable Isotopes (C18:1ω7 (‰) vs. C20:1 (‰)) of fatty acids at the downstream site.

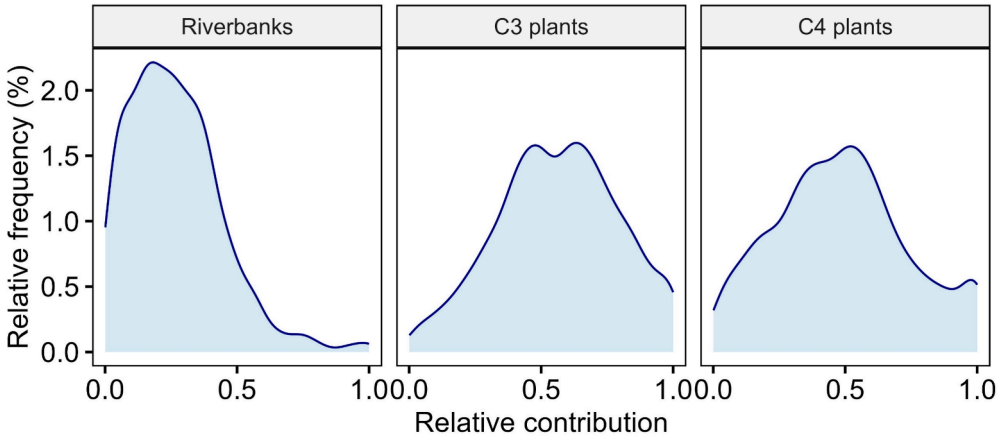

Fig. 4. Frequency distributions of relative sediment contributions using compound-specific stable isotopes of fatty acids at the midstream site.

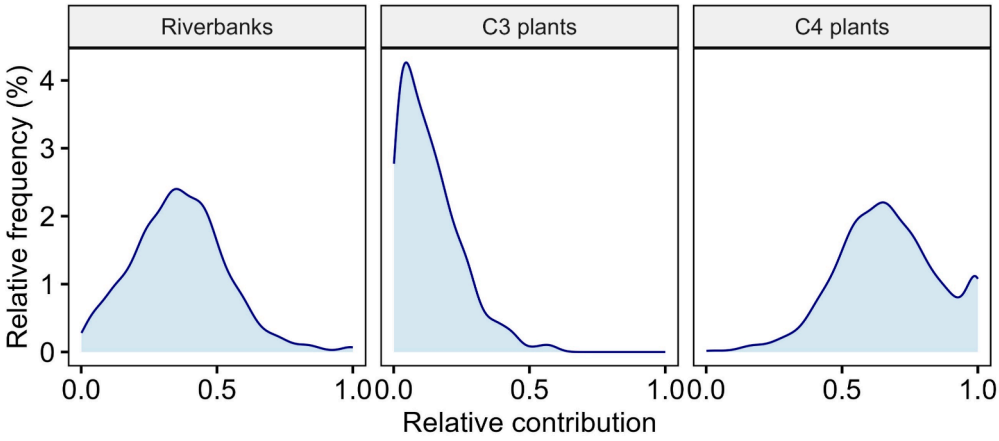

Fig. 5. Frequency distributions of relative sediment contributions using compound-specific stable isotopes of fatty acids at the downstream site.

3.1.2. *Identification of sediment sources*

The relative contribution of sediment from C3 plants, C4 plants, and riverbanks at the midstream and downstream sites of the Geesgraben catchment was estimated based on compound-specific stable isotope tracers (CSSIs) selected using the Kruskal-Wallis test and discriminant function analysis. At the midstream site, the relative contribution of sediment from C3 plants, C4 plants, and riverbanks was 44 %, 44 %, and 12 %, respectively estimated using C20:1, and C23:0 in the multivariate mixing model. The goodness-of-fit of the model was 99.9 % (Fig. 4). The different shapes of the probability distribution functions for riverbanks, C3, and C4 plants give different mean contributions of the sediment sources.

At the downstream site, the relative contribution from C3 plants, C4 plants, and riverbanks was 9 %, 63 %, and 28 %, respectively estimated using C18:1ω7, and C20:1 in the multivariate mixing model. The goodness-of-fit of the model was 99.9 % (Fig. 5). The results at the downstream site are better than those generated at the midstream site from the CSSIs tracers as the mixing model output probability density functions are more leptokurtic (peakier). This reflects the improved source discrimination using CSSI tracers at the outlet. Comparison between the riverbank source apportionment results generated at the midstream and downstream sites suggested different mean contributions. This is also reflected by having different shapes of the probability distribution functions.

3.2. *Identification of surface and riverbank sources*

3.2.1. *Identification of sources using radionuclide tracers*

The final radionuclide tracers were selected using the F-ratio and range test. Second, the final set of tracers with high discrimination power was selected using the Kruskal-Wallis test ($P < 0.05$) and DFA (level < 0.1) (Table 7) for campaigns 1, and 2 for the mixing model. In the end, only $^{210}Pb_{ex}$ and ^{137}Cs were selected for sediment source estimations. See Table S4 for the concentration of radionuclide tracers, number of samples, mean, and the coefficient of variation for arable land and riverbanks.

After the two-step screening procedure, the Kruskal-Wallis test, and DFA, biplot (Fig. 6) provided further evidence of the conservative

Table 7
Radionuclide tracers selected using the ANOVA F-ratio, range test, Kruskal-Wallis test (asterisks, $P < 0.05$), and discriminant function analysis (asterisks, level < 0.1).

Campaign	Tracers	F-ratio	Within range	H statistics	P value	Wilks lambda	F statistics	level
1	^{137}Cs	30.1	^{137}Cs	22.4	< 0.05*	0.62	30.1	< 0.1*
	$^{210}Pb_{ex}$	4.80	$^{210}Pb_{ex}$	4.79	< 0.05*	0.91	4.80	< 0.1*
2	^{137}Cs	30.2	^{137}Cs	22.4	< 0.05*	0.62	30.2	< 0.1*
	$^{210}Pb_{ex}$	4.90	$^{210}Pb_{ex}$	4.79	< 0.05*	0.91	4.90	< 0.1*

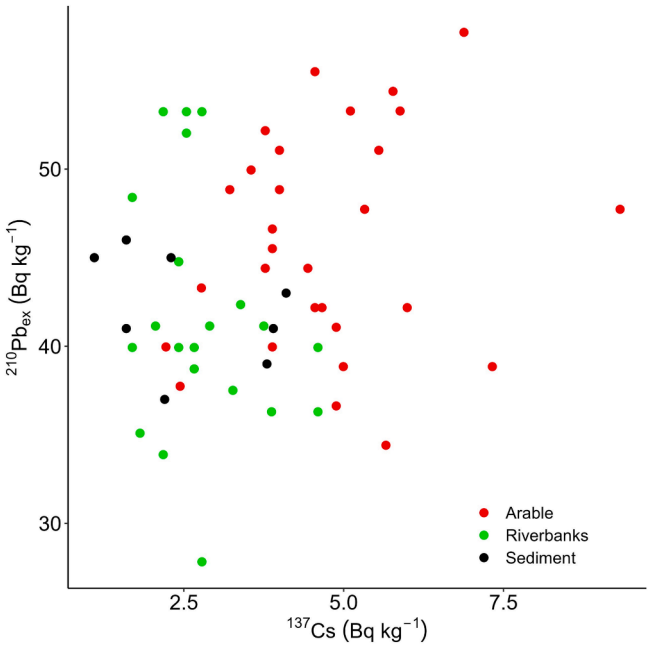

Fig. 6. Biplot of radionuclide concentrations at the downstream site.

behavior, because the soil and sediment samples were plotted along the same lines or in the same space.

The biplot showed consistent results for ^{137}Cs and excess $^{210}Pb_{ex}$, although riverbanks showed some high scatter for the sediment samples. The two sediment samples from the biplot for ^{137}Cs and excess $^{210}Pb_{ex}$ of soil and sediment samples for campaigns 1 and 2 were selected at the downstream site. Two radionuclide tracers (^{137}Cs and $^{210}Pb_{ex}$) were used in each campaign 1, and 2 in the mixing model. The main sediment source in campaigns 1 and 2 was arable land (59 % and 79 %, respectively), which was higher than the contribution of riverbanks (41 % and 21 %, respectively). The mean concentration of $^{210}Pb_{ex}$ between the sources was not statistically different in campaign 3, we need at least two tracers in the mixing model for estimation of relative source estimation, therefore, excluded campaign 3 for further analysis. The sediment sources did not shift greatly between campaigns 1 and 2, which were performed in different seasons of the year. The GOF of the mixing model for both campaigns was 99 %. The main sediment source from campaign 1 was arable land, which was similar to the estimates obtained using CSSIs.

3.2.2. *Identifying sources based on spectral properties*

Spectral properties, including color-based parameters (Table S5) and physically based spectral features (Table S6), were used to distinguish sediment sources. See Table S7 for the values of spectral properties, number of samples, mean, and coefficient of variation for the sources and sediments. The final set of properties was selected based on the Kruskal-Wallis test ($P < 0.05$) (Tables S8 and S9) for campaigns 1 and 2 respectively, and DFA (level < 0.1) (Table S10) for both campaigns. Biplots (Fig. S1 and S2 for campaign 1 while Fig. S3 for campaign 2) gave further evidence for the conservative behavior of spectral property concentrations.

The spectral properties also showed that sediment came mainly from the arable land (90–97 %), while the riverbanks contributed only 3–10 % (Table 8), which does not agree with the results of the other fingerprinting methods used (i.e., radionuclide and CSSI). The mean estimated sediment contribution from arable land was 90 % for campaign 1 and 97 % for campaign 2, which showed that there was no difference within the year. The spectral properties in campaign 3 give a 1 % source contribution from arable land which was not the case in the catchment although have 81 % model performance, recent research gives evidence that the model with high goodness-of-fit can still estimate inaccurate outcomes (Palazón et al., 2015), we do not see any difference between the campaigns and besides the radionuclide tracers were not worked for comparison therefore excluded campaign 3 from further comparison study. The spectral properties showed little deviation in outcomes than the other fingerprinting methods used.

4. Discussion

4.1. *Upland erosion and sediment contribution from specific crop types and riverbanks*

While plot-scale studies provide information about erosion processes and nutrient and soil losses under different crop types, they provide no information about sediment load at a catchment outlet (Walling, 1983). The $\delta^{13}C$-CSSIs of FAs can fill this knowledge gap by estimating crop-specific sediment loads at the catchment scale (Blake et al., 2012). Our findings from the outlet of the Geesgraben catchment demonstrate that C4 plants contributed more sediment (63 %) than C3 plants (9 %), even though C4 crops (16 %) covered much less of the catchment than C3 crops (61 %) did. The sediment contribution from C4 plants at the outlet was due to a higher upland erosion rate compared to C3 plants. Similarly, at the midstream site C3 and C4 plants contributed 44 % each, and riverbanks contributed 12 % of sediment at the midstream site, which was lower than the 28 % contributed at the downstream site. The mean upland erosion rates from C3 and C4 plants using the RUSLE model were 0.63 t ha^{-1} yr^{-1} and 1.58 t ha^{-1} yr^{-1} respectively. The percentage contribution of total soil erosion from C3 and C4 plants by the RUSLE model was 29 % and 71 % respectively. These numbers are in a similar range to the CSSI calculated share of C3 and C4 sediment sources on total upland erosion (12.5 % and 87.5 %, respectively). The CSSI fingerprinting method and RUSLE model show comparable results in our catchment. The findings from the two different methods of CSSI fingerprinting and the RUSLE model do not indicate that sediment connectivity largely impacts the shares of C3 and C4 cropping areas on sediment load from this catchment. This corroborate also findings from the United Kingdom (UK) which showed that winter wheat (C3) generally had a lower erosion risk than maize (C4) (Evans, 2005). In addition, during sampling campaigns, most fields were covered with wheat to maximize crop cover to reduce rainfall-induced soil erosion (Evans, 2005). Withers et al. (2007) reasoned that the timing of sowing winter wheat is important to maximize crop cover during peak rainfall events. Information about the specific crops and sediment sources in a catchment is necessary to understand the on– and off-site impacts of soil erosion accelerated by agricultural use, which highlights the importance of agricultural practices. Thus, in the Geesgraben catchment and areas with similar site characteristics, erosion-mitigation measures should focus mainly on proper maize-management strategies to reduce soil erosion and sediment load.

Most loess areas are either flat or hilly locally and thus have similar physical and chemical properties. The mean arable upland erosion rate in the Geesgraben catchment was 0.84 t ha^{-1} yr^{-1}, with a riverbank contribution of 3–41 % estimated using three fingerprinting methods.

Table 8
Relative contribution of surface and riverbanks to sediment sources in the Geesgraben catchment using spectral properties for campaigns 1 and 2. GOF: goodness-of-fit.

Method	Campaign	GOF	Riverbanks	Arable	Final selection
Spectral properties	**1**	80 %	10 %	90 %	*CIE.H, H, AF1 AS, AF4 w, AF6 AS, AF13 w*
	2	91 %	3 %	97 %	*CIE.H, H, AF4 w, AF5 w*

The sediment load at the outlet was 0.12 t ha^{-1} yr^{-1}, with a delivery ratio of 14 %. The upland erosion predicted by RUSLE represents only the displacement of soil loss from one area to another and does not represent sediment transport to streams. In contrast, CSSIs and other fingerprinting methods estimate relative contributions to sediment loads from sources to streams. The River Ouse (3315 km^2), in a temperate region (UK) with predominantly agricultural land use, had a riverbank contribution of 37 % and an upland erosion rate of 1.05 t ha^{-1} yr^{-1} (Walling et al., 1999), which were similar to those of the Geesgraben catchment. The Swale (1346 km^2) and Nidd (484 km^2) subcatchments of the River Ouse, which have similar geology and topography, also had similar upland erosion rates (0.94 t ha^{-1} yr^{-1} each), and their riverbank contribution was 28 % and 15 %, respectively (Walling et al., 1999), which were also similar to those of the Geesgraben catchment. Similarly, the Avon (324 km^2), Wylye (446 km^2), and Lower Avon (1477 km^2) catchments in the UK had an upland erosion rate of 0.71–1.07 t ha^{-1} yr^{-1}, a mean riverbank contribution of 13 %, and a cropland contribution of 72 % (Heywood, 2002). Most of the sediments from these catchments were delivered from the agricultural source (pasture and cropland) contributing 63–90 % of the total loads. The major land use was grassland (41.4–50.5 %) and arable land use (18.7–38.9 %). These catchments have a similar range of riverbank sediment contributions (8.2–37 %) and a similar range of upland erosion rates (0.71–1.07 t ha^{-1} yr^{-1}) regardless of catchment size (Heywood, 2002; Walling et al., 1999). The riverbank contribution in other UK catchments was 12 %, with an upland erosion rate of 1.05 t ha^{-1} yr^{-1} (Collins et al., 1997a). These results indicate that loess-soil catchments can have source contributions similar to those of non-loess soil catchments.

In the present study, riverbanks contributed more sediment at the outlet than in the headwater. Likewise, Lawler et al. (1999) observed an apparent downstream increase in riverbank erosion. The riverbank contribution also followed a similar trend in the River Ouse (which had similar land uses) and increased as catchment size increased (Walling et al., 1999). In another study, sediment sources shifted from the surface to riverbanks in the downstream direction (Heywood, 2002). A recent study found that, as catchment size increased, sediment loads from the surface decreased and the relative riverbank contribution increased downstream (Abbas et al., 2023). This information is crucial for the management strategies of stakeholders; management practices should focus on downstream sections to stabilize riverbanks in order to decrease sediment loads at the catchment scale.

Riparian vegetation extends along some of the riverbanks from the upstream to downstream sites in the Geesgraben catchment, which helps decrease riverbank erosion and sediment transfer. Riparian forests are largely absent from low-order agricultural streams, but they could increase riverbank stability by increasing soil shear strength and reinforcing the riverbank (Abernethy and Rutherfurd, 1998; Thorne and Tovey, 1981). Revegetation could be the most effective approach for reducing riverbank erosion in high-erosion areas (Abernethy and Rutherfurd, 1998). Moreover, riparian vegetation, artificial ponds, and wetlands decrease connectivity among sediment sources and rivers and help trap sediment (Tiecher et al., 2017). Proper management of agricultural land use practices (e.g., terracing) can decrease sediment transport and delivery (Upadhayay et al., 2018). The δ^{13}C-CSSIs of FAs thus act like a tool that stakeholders can use to modify land use practices and apply new strategies for decreasing sediment transport to river ecosystems and estuaries (Gibbs, 2008).

4.2. Comparison of fingerprinting methods

The δ^{13}C-CSSIs of FAs were used to investigate the riverbank contribution to the total sediment load at the catchment scale and found that arable land was the main source of sediment. The contribution from riverbanks estimated using δ^{13}C-FAs, radionuclide tracers, and spectral properties differed distinctly and ranged from 3-41 % at the downstream site.

Although all methods (CSSI, radionuclide, and spectral) revealed a higher percentage of upland contribution than riverbank contribution, the methods differ in several aspects. Results of the CSSI and radionuclide methods were more similar to each other than to those of the spectral method. The GOF of the mixing model was high and similar for the CSSI and radionuclide methods but lower for the spectral method; thus, the spectral results were less reliable for this catchment. Previous studies have also compared fingerprinting methods and successfully used δ^{13}C-CSSIs of FAs to identify sediment sources, and their results were similar to and consistent with those of other fallout radionuclides and elemental geochemistry (Hancock and Revill, 2013). However, radionuclide tracers could not distinguish forest and pasture sources and can also fail to distinguish riverbank and hillslope B-horizon sources if these two sources have similar distributions of radionuclide concentrations. In contrast, CSSIs can distinguish surface (e.g., forest, pasture) and subsurface sources (e.g., riverbanks, hillslope B-horizons) (Hancock and Revill, 2013). CSSIs can also distinguish cropped soils when crops are harvested over a long period (Hancock and Revill, 2013). Another study that compared CSSI and geochemical fingerprinting found that soil organic matter from weeds can influence bulk δ^{13}C signatures; thus, the CSSI method requires careful application when soil organic matter content varies (Blake et al., 2012). In contrast, a study that compared radionuclide and geochemical fingerprinting methods found similar and consistent results for the contribution of surface and subsurface sources (Rode et al., 2018).

The use of radionuclides has specific advantages, such as high sensitivity and the ability to trace recently displaced sediment. However, because riverbank and gully soils have little or no ^{137}Cs and excess ^{210}Pb$_{ex}$, the use of radionuclides has some limitations (Hancock and Revill, 2013). Radionuclides also have little ability to assess the contribution of different sediment sources that could be deposited or accumulated in the landscape (Blake et al., 2012; Guzmán et al., 2013). Due to a low proportion of radioactive fallout in areas ranging from 20°S-20°N, the use of ^{137}Cs can be limited. Moreover, radioactive fallout continues to decay until its concentration falls below the detection threshold. For this reason, other fingerprinting methods should be included to obtain more reliable results (Evrard et al., 2020). The use of radionuclides requires careful sampling campaigns and laboratory analysis, especially for radionuclides with a short half-life (e.g., 53 days for beryllium). Consequently, radionuclide fingerprinting may sometimes not show conservativeness in the final calculation (Hancock et al., 2014). We planned to examine beryllium in the present study, but because the COVID-19 pandemic delayed laboratory analysis, no beryllium could be detected in the soil or sediment samples. Nonetheless, depending on the soil type, radionuclides remain useful for distinguishing surface and subsurface sources, since they are not influenced by soil type or lithology, which allows radionuclides to be used in heterogeneous catchments where other tracers may be of limited use (Walling and Woodward, 1992).

The use of sediment-source fingerprinting is not widespread due to the cost and effort involved in preparing samples for radionuclide and elemental geochemistry analysis. In comparison, spectral fingerprinting can be a rapid and cost-effective alternative (Brosinsky et al., 2014b). In addition to having less labor-intensive laboratory analysis, spectroscopy requires only small sample sizes (Martínez-Carreras et al., 2010), but spectral properties require careful consideration due to the method's high variability and uncertainty. In the present study, the high uncertainty and variability in the spectral properties resulted in a low GOF and were ultimately similar to those of the radionuclide and CSSI methods. Researchers can use spectral properties to distinguish sediment sources by considering a few recommendations in order to provide information for environmental decision-making strategies. The effectiveness of the spectral method can be increased by calibrating it using known sediment mixtures to estimate relations between spectral signatures and sediment-source percentages. In addition, conventional and alternative properties can be combined to improve the identification of

sediment sources and optimize model results (Collins and Walling, 2002).

Geochemical tracers were also tested in the present study's loess-soil subcatchments, but could not be successfully applied, since the geochemical characteristics of the potential sediment sources differed little. This was confirmed by the low GOF of the mixing model that considered soil geochemistry, which was based on differences in the chemical composition of potential sediment sources. These results for the Geesgraben catchment indicated that these small differences could limit the effectiveness of geochemical tracers in loess-soil catchments, which thus requires investigating alternative methods. In this situation, other fingerprinting properties such as radionuclides, spectral, and δ^{13}C-CSSIs of FAs can help distinguish sources.

The fingerprinting method(s) to select depends on catchment characteristics, resource availability, and specific research questions. Distinguishing sediment sources that are physically and chemically similar can become challenging when using conventional methods alone. The CSSI method can distinguish sources that may appear relatively similar, such as riverbanks and hillslope B-horizons, but that have distinct isotopic signatures. The CSSI method does not involve radioactive materials, which makes it environmentally friendly and ensures safe and more accessible analysis, and is not limited to specific geographic regions or types of sediments. The CSSI method successfully distinguished surface and subsurface sources, suggesting that it can be used to identify sediment sources (Blake et al., 2012). It can also be used to identify sediment sources based on a sediment connectivity index, since higher connectivity increases contribution to the sediment at the catchment outlet (Upadhayay et al., 2020). Based on the results of our study, the CSSI method is preferable and highly recommended for distinguishing sediment sources at the catchment scale compared to the radionuclide and spectral methods. CSSI fingerprinting may also need to be applied over long periods to interpret seasonal differences in sediment sources, which can change during extreme events and thus require long-term and spatial assessment of the dynamics of sediment sources.

5. Conclusion

Few studies have applied δ^{13}C-CSSIs of FAs at the catchment scale to identify suspended-sediment sources from C3 and C4 plants and riverbanks. This novel technique uses δ^{13}C-FAs to distinguish the specific land use types (e.g., C3 and C4 plants) that contribute to the sediment load. These tracers were also successfully used to distinguish the surface (arable) and subsurface (riverbanks) sources of sediment in the loess-soil catchment studied. The relative contributions of arable land and riverbanks estimated by the CSSI method were similar to or partially consistent with those of the radionuclide and spectral methods, respectively. The results showed that a disproportionate percentage of the total sediment load came from areas with maize (C4 crop), which has high erodibility. Measures to reduce the sediment load from loess areas should thus focus first on C4 crops. In addition, riverbank erosion also represented a substantial percentage of the total sediment load in the catchment. Thus, measures to decrease sediment discharge in loess areas should not concentrate only on decreasing upland erosion, but should also decrease riverbank erosion, such as by protecting riverbanks with riparian forest strips.

CRediT authorship contribution statement

Ghulam Abbas: Writing – original draft, Methodology, Formal analysis, Data curation, Conceptualization. **Seifeddine Jomaa:** Writing – review & editing, Supervision, Conceptualization. **Patrick Fink:** Writing – review & editing, Supervision, Investigation. **Arlena Brosinsky:** Writing – review & editing, Supervision, Formal analysis. **Karolina Malgorzata Nowak:** Writing – review & editing, Supervision, Investigation. **Steffen Kümmel:** Writing – review & editing, Supervision, Investigation. **Uwe-Karsten Schkade:** Investigation, Formal analysis. **Michael Rode:** Writing – review & editing, Supervision, Resources, Investigation, Funding acquisition, Conceptualization.

Declaration of competing interest

The authors declare the following financial interests/personal relationships which may be considered as potential competing interests: [Ghulam Abbas reports financial support, administrative support, article publishing charges, travel, and writing assistance were provided by Helmholtz-Centre for Environmental Research – UFZ. If there are other authors, they declare that they have no known competing financial interests or personal relationships that could have appeared to influence the work reported in this paper].

Data availability

Data will be made available on request.

Acknowledgment

The authors express gratitude to the Higher Education Commission of Pakistan (HEC) for the scholarship funds jointly provided by the German Academic Exchange Service (DAAD). We would like to thank Uwe Kiwel for their assistance within the expeditions and Wolf von Tümpling, Andrea Hoff, and Ines Locker for laboratory analysis. The generous help of landowners in granting access to field and river sampling sites. We thank Gunnar Pruss for his assistance in particle size distribution in Section 4.6: Geomorphology for SedLab: Grain size measurements (Retsch LA950). The authors are also grateful for the use of the analytical facilities of the Laboratories for Stable Isotopes (LSI) at the Helmholtz Centre for Environmental Research. We would also like to thank the reviewers for their insightful feedback.

Appendix A. Supplementary data

Supplementary data to this article can be found online at https://doi.org/10.1016/j.catena.2024.108336.

References

Abbas, G., Jomaa, S., Bronstert, A., Rode, M., 2023. Downstream changes in riverbank sediment sources and the effect of catchment size. J. Hydrol.: Reg. Stud. 46, 101340 https://doi.org/10.1016/j.ejrh.2023.101340.

Abernethy, B., Rutherfurd, I.D., 1998. Where along a river's length will vegetation most effectively stabilise stream banks? Geomorphology 23 (1), 55–75. https://doi.org/10.1016/S0169-555X(97)00089-5.

Auerswald, K., Fischer, F.K., Winterrath, T., Brandhuber, R., 2019. Rain erosivity map for Germany derived from contiguous radar rain data. Hydrol. Earth Syst. Sci. 23 (4), 1819–1832. https://doi.org/10.5194/hess-23-1819-2019.

Bayer, A., Bachmann, M., Müller, A., Kaufmann, H., 2012. A Comparison of feature-based MLR and PLS regression techniques for the prediction of three soil constituents in a degraded South African Ecosystem. Appl. Environ. Soil Sci. 2012 (1), 971252 https://doi.org/10.1155/2012/971252.

Blake, W.H., Ficken, K.J., Taylor, P., Russell, M.A., Walling, D.E., 2012. Tracing crop-specific sediment sources in agricultural catchments. Geomorphology 139–140, 322–329. https://doi.org/10.1016/j.geomorph.2011.10.036.

Brandt, C., Cadisch, G., Nguyen, L.T., Vien, T.D., Rasche, F., 2016. Compound-specific δ^{13}C isotopes and Bayesian inference for erosion estimates under different land use in Vietnam. Geoderma Reg. 7 (3), 311–322. https://doi.org/10.1016/j.geodrs.2016.06.001.

Brandt, C., Benmansour, M., Walz, L., Nguyen, L.T., Cadisch, G., Rasche, F., 2018a. Integrating compound-specific δ^{13}C isotopes and fallout radionuclides to retrace land use type-specific net erosion rates in a small tropical catchment exposed to intense land use change. Geoderma 310, 53–64. https://doi.org/10.1016/j.geoderma.2017.09.008.

Brandt, C., Dercon, G., Cadisch, G., Nguyen, L.T., Schuller, P., Linares, C.B., Santana, A. C., Golosov, V., Benmansour, M., Amenzou, N., Xinbao, Z., Rasche, F., 2018b. Towards global applicability? Erosion source discrimination across catchments using compound-specific δ^{13}C isotopes. Agr Ecosyst Environ 256, 114–122. https://doi.org/10.1016/j.agee.2018.01.010.

Brosinsky, A., Foerster, S., Segl, K., Kaufmann, H., 2014a. Spectral fingerprinting: sediment source discrimination and contribution modelling of artificial mixtures based on VNIR-SWIR spectral properties. J. Soil. Sediment. 14, 1949–1964. https://doi.org/10.1007/s11368-014-0925-1.

Brosinsky, A., Foerster, S., Segl, K., López-Tarazón, J.A., Piqué, G., Bronstert, A., 2014b. Spectral fingerprinting: characterizing suspended sediment sources by the use of VNIR-SWIR spectral information. J. Soil. Sediment. 14, 1965–1981. https://doi.org/10.1007/s11368-014-0927-z.

Cerdan, O., Govers, G., Le Bissonnais, Y., Van Oost, K., Poesen, J., Saby, N., Gobin, A., Vacca, A., Quinton, J., Auerswald, K., Klik, A., Kwaad, F.J.P.M., Raclot, D., Ionita, I., Rejman, J., Rousseva, S., Muxart, T., Roxo, M.J., Dostal, T., 2010. Rates and spatial variations of soil erosion in Europe: a study based on erosion plot data. Geomorphology 122 (1–2), 167–177. https://doi.org/10.1016/j.geomorph.2010.06.011.

Chabrillat, S., Eisele, A., Guillaso, S., Rogaß, C., Ben-Dor, E., Kaufmann, H. (2011). HYSOMA: An easy-to-use software interface for soil mapping applications of hyperspectral imagery. *7th EARSeL SIG Imaging Spectroscopy Workshop, Edinburgh, Scotland*.

Collins, A.L., Walling, D.E., Leeks, G.J.L., 1997b. Source type ascription for fluvial suspended sediment based on a quantitative composite fingerprinting technique. Catena 29 (1), 1–27. https://doi.org/10.1016/S0341-8162(96)00064-1.

Collins, A.L., Walling, D.E., 2002. Selecting fingerprint properties for discriminating potential suspended sediment sources in river basins. J. Hydrol. 261 (1–4), 218–244. https://doi.org/10.1016/S0022-1694(02)00011-2.

Collins, A.L., Walling, D.E., Leeks, G.J.L., 1997a. Sediment sources in the Upper Severn catchment: a fingerprinting approach. Hydrol. Earth Syst. Sci. 1 (3), 509–521. https://doi.org/10.5194/hess-1-509-1997.

Evans, R., 2005. Monitoring water erosion in lowland England and Wales—a personal view of its history and outcomes. Catena 64 (2–3), 142–161. https://doi.org/10.1016/j.catena.2005.08.003.

Evrard, O., Laceby, J.P., Ficetola, G.F., Gielly, L., Huon, S., Lefèvre, I., Onda, Y., Poulenard, J., 2019. Environmental DNA provides information on sediment sources: a study in catchments affected by Fukushima radioactive fallout. Sci. Total Environ. 665, 873–881. https://doi.org/10.1016/j.scitotenv.2019.02.191.

Evrard, O., Chaboche, P.A., Ramon, R., Foucher, A., Laceby, J.P., 2020. A global review of sediment source fingerprinting research incorporating fallout radiocesium (^{137}Cs). Geomorphology 362, 107103. https://doi.org/10.1016/j.geomorph.2020.107103.

Gellis, A.C., Fuller, C.C., Van Metre, P.C., 2017. Sources and ages of fine-grained sediment to streams using fallout radionuclides in the Midwestern United States. J. Environ. Manage. 194, 73–85. https://doi.org/10.1016/j.jenvman.2016.06.018.

Gibbs, M.M., 2008. Identifying source soils in contemporary estuarine sediments: a new compound-specific isotope method. Estuar. Coasts 31, 344–359. https://doi.org/10.1007/s12237-007-9012-9.

Guzmán, G., Quinton, J.N., Nearing, M.A., Mabit, L., Gómez, J.A., 2013. Sediment tracers in water erosion studies: current approaches and challenges. J. Soil. Sediment. 13, 816–833. https://doi.org/10.1007/s11368-013-0659-5.

Hancock, G.J., Revill, A.T., 2013. Erosion source discrimination in a rural Australian catchment using compound-specific isotope analysis (CSIA). Hydrol. Process. 27 (6), 923–932. https://doi.org/10.1002/hyp.9466.

Hancock, G.J., Wilkinson, S.N., Hawdon, A.A., Keen, R.J., 2014. Use of fallout tracers ^{7}Be, ^{210}Pb and ^{137}Cs to distinguish the form of sub-surface soil erosion delivering sediment to rivers in large catchments. Hydrol. Process. 28 (12), 3855–3874. https://doi.org/10.1002/hyp.9926.

Heywood, M. J. T. (2002). Sedimentation of salmonid spawning gravels: an investigation of associated sediment dynamics in the Hampshire Avon catchment. *Doctoral Dissertation, University of Exeter*.

Hooke, R.L., Martín-Duque, J.F., Pedraza, J., 2012. Land transformation by humans: a review. GSA Today 22 (12), 4–10. https://doi.org/10.1130/GSAT151A.1.

Jeffries, R., Darby, S.E., Sear, D.A., 2003. The influence of vegetation and organic debris on flood-plain sediment dynamics: case study of a low-order stream in the New Forest England. Geomorphology 51 (1–3), 61–80. https://doi.org/10.1016/S0169-555X(02)00325-2.

Lawler, D.M., Grove, J.R., Couperthwaite, J.S., Leeks, G.J.L., 1999. Downstream change in river bank erosion rates in the Swale-Ouse system, northern England. Hydrol. Process. 13 (7), 977–992. https://doi.org/10.1002/(SICI)1099-1085(199905)13:7<977::AID-HYP785>3.0.CO;2-5.

Lizaga, I., Latorre, B., Gaspar, L., Navas, A., 2020. FingerPro: an R package for tracking the provenance of sediment. Water Resour. Manag. 34 (12), 3879–3894. https://doi.org/10.1007/s11269-020-02650-0.

Mabit, L., Gibbs, M., Mbaye, M., Meusburger, K., Toloza, A., Resch, C., Klik, A., Swales, A., Alewell, C., 2018. Novel application of Compound Specific Stable Isotope (CSSI) techniques to investigate on-site sediment origins across arable fields. Geoderma 316, 19–26. https://doi.org/10.1016/j.geoderma.2017.12.008.

Martínez-Carreras, N., Udelhoven, T., Krein, A., Gallart, F., Iffly, J.F., Ziebel, J., Hoffmann, L., Pfister, L., Walling, D.E., 2010. The use of sediment colour measured by diffuse reflectance spectrometry to determine sediment sources: application to the attert river catchment (Luxembourg). J. Hydrol. 382 (1–4), 49–63. https://doi.org/10.1016/j.jhydrol.2009.12.017.

Nowak, K.M., Miltner, A., Gehre, M., Schäffer, A., Kästner, M., 2011. Formation and fate of bound residues from microbial biomass during 2, 4-D degradation in soil. Environ. Sci. Tech. 45 (3), 999–1006. https://doi.org/10.1021/es103097f.

Owens, P.N., Walling, D.E., Leeks, G.J.L., 2000. Tracing fluvial suspended sediment sources in the catchment of the River Tweed, Scotland, using composite fingerprints and a numerical mixing model. Tracers in Geomorphology 291–308.

Owens, P.N., Blake, W.H., Gaspar, L., Gateuille, D., Koiter, A.J., Lobb, D.A., Petticrew, E. L., Reiffarth, D.G., Smith, H.G., Woodward, J.C., 2016. Fingerprinting and tracing the sources of soils and sediments: earth and ocean science, geoarchaeological, forensic, and human health applications. Earth Sci. Rev. 162, 1–23. https://doi.org/10.1016/j.earscirev.2016.08.012.

Palazón, L., Latorre, B., Gaspar, L., Blake, W.H., Smith, H.G., Navas, A., 2015. Comparing catchment sediment fingerprinting procedures using an auto-evaluation approach with virtual sample mixtures. Sci. Total Environ. 532, 456–466. https://doi.org/10.1016/j.scitotenv.2015.05.003.

Preidl, S., Lange, M., Doktor, D., 2020. Introducing APiC for regionalised land cover mapping on the national scale using Sentinel-2A imagery. Remote Sens. Environ. 240, 111673 https://doi.org/10.1016/j.rse.2020.111673.

Reiffarth, D.G., Petticrew, E.L., Owens, P.N., Lobb, D.A., 2016. Sources of variability in fatty acid (FA) biomarkers in the application of compound-specific stable isotopes (CSSIs) to soil and sediment fingerprinting and tracing: a review. Sci. Total Environ. 565, 8–27. https://doi.org/10.1016/j.scitotenv.2016.04.137.

Renard, K.G., Foster, G.R., Weesies, G.A., McCool, D.K., Yoder, D.C., 1996. Predicting soil erosion by water: A guide to conservation planning with the Revised Universal Soil Loss Equation (RUSLE). USDA-Agricultural Research Service, Agriculture Handbook Number, p. 703.

Rode, M., op de Hipt, F., Collins, A.L., Zhang, Y., Theuring, P., Schkade, U.K., Diekkrüger, B., 2018. Subsurface sources contribute substantially to fine-grained suspended sediment transported in a tropical West African watershed in Burkina Faso. Land Degrad. Dev. 29 (11), 4092–4105. https://doi.org/10.1002/ldr.3165.

Russell, M.A., Walling, D.E., Hodgkinson, R.A., 2001. Suspended sediment sources in two small lowland agricultural catchments in the UK. J. Hydrol. 252 (1–4), 1–24. https://doi.org/10.1016/S0022-1694(01)00388-2.

Schwertmann, U., Vogl, W., & Kainz, M. (1987). Bodenerosion durch Wasser. *Ulmer Verlag, 64p*.

Theuring, P., Rode, M., Behrens, S., Kirchner, G., Jha, A., 2013. Identification of fluvial sediment sources in the Kharaa River catchment, Northern Mongolia. Hydrol. Process. 27 (6), 845–856. https://doi.org/10.1002/hyp.9684.

Theuring, P., Collins, A.L., Rode, M., 2015. Source identification of fine-grained suspended sediment in the Kharaa River basin, northern Mongolia. Sci. Total Environ. 526, 77–87. https://doi.org/10.1016/j.scitotenv.2015.03.134.

Thorne, C.R., Tovey, N.K., 1981. Stability of composite river banks. Earth Surf. Proc. Land. 6 (5), 469–484. https://doi.org/10.1002/esp.3290060507.

Tiecher, T., Caner, L., Minella, J.P.G., Pellegrini, A., Capoane, V., Rasche, J.W.A., Schaefer, G.L., dos Santos Rheinheimer, D., 2017. Tracing sediment sources in two paired agricultural catchments with different riparian forest and wetland proportion in southern Brazil. Geoderma 285, 225–239. https://doi.org/10.1016/j.geoderma.2016.10.008.

Upadhayay, H.R., Bodé, S., Griepentrog, M., Huygens, D., Bajracharya, R.M., Blake, W. H., Dercon, G., Mabit, L., Gibbs, M., Semmens, B.X., Stock, B.C., Cornelis, W., Boeckx, P., 2017. Methodological perspectives on the application of compound-specific stable isotope fingerprinting for sediment source apportionment. J. Soil. Sediment. 17, 1537–1553. https://doi.org/10.1007/s11368-017-1706-4.

Upadhayay, H.R., Smith, H.G., Griepentrog, M., Bodé, S., Bajracharya, R.M., Blake, W., Cornelis, W., Boeckx, P., 2018. Community managed forests dominate the catchment sediment cascade in the mid-hills of Nepal: a compound-specific stable isotope analysis. Sci. Total Environ. 637–638, 306–317. https://doi.org/10.1016/j.scitotenv.2018.04.394.

Upadhayay, H.R., Lamichhane, S., Bajracharya, R.M., Cornelis, W., Collins, A.L., Boeckx, P., 2020. Sensitivity of source apportionment predicted by a Bayesian tracer mixing model to the inclusion of a sediment connectivity index as an informative prior: Illustration using the Kharka catchment (Nepal). Sci. Total Environ. 713, 136703 https://doi.org/10.1016/j.scitotenv.2020.136703.

Valente, M.L., Reichert, J.M., Legout, C., Tiecher, T., Cavalcante, R.B.L., Evrard, O., 2020. Quantification of sediment source contributions in two paired catchments of the Brazilian Pampa using conventional and alternative fingerprinting approaches. Hydrol. Process. 34 (13), 2965–2986. https://doi.org/10.1002/hyp.13768.

Viscarra Rossel, R.A., Walvoort, D.J.J., McBratney, A.B., Janik, L.J., Skjemstad, J.O., 2006. Visible, near infrared, mid infrared or combined diffuse reflectance spectroscopy for simultaneous assessment of various soil properties. Geoderma 131 (1–2), 59–75. https://doi.org/10.1016/j.geoderma.2005.03.007.

Walling, D.E., 1983. The sediment delivery problem. J. Hydrol. 65 (1–3), 209–237. https://doi.org/10.1016/0022-1694(83)90217-2.

Walling, D.E., 1999. Linking land use, erosion and sediment yields in river basins. Hydrobiologia 410, 223–240. https://doi.org/10.1023/A:1003825813091.

Walling, D.E., Collins, A.L., 2005. Suspended sediment sources in British rivers. Sediment Budgets, IAHS Publication 291, 123–133.

Walling, D.E., Owens, P.N., Leeks, G.J.L., 1999. Fingerprinting suspended sediment sources in the catchment of the River Ouse, Yorkshire UK. Hydrol. Process. 13 (7), 955–975. https://doi.org/10.1002/(SICI)1099-1085(199905)13:7<955::AID-HYP784>3.0.CO;2-G.

Walling, D.E., Woodward, J.C., 1992. Use of radiometric fingerprints to derive information on suspended sediment sources. Erosion and Sediment Transport Monitoring Programmes in River Basins, IAHS Publ. 210, 153–164.

Walling, D.E., Woodward, J.C., 1995. Tracing sources of suspended sediment in river basins: a case study of the River Culm, Devon UK. Mar. Freshw. Res. 46 (1), 327–336. https://doi.org/10.1071/MF9950327.

Wethered, A.S., Ralph, T.J., Smith, H.G., Fryirs, K.A., Heijnis, H., 2015. Quantifying fluvial (dis)connectivity in an agricultural catchment using a geomorphic approach and sediment source tracing. J. Soil. Sediment. 15, 2052–2066. https://doi.org/10.1007/s11368-015-1202-7.

Withers, P.J.A., Hodgkinson, R.A., Bates, A., Withers, C.L., 2007. Soil cultivation effects on sediment and phosphorus mobilization in surface runoff from three contrasting soil types in England. Soil Tillage Res. 93 (2), 438–451. https://doi.org/10.1016/j.still.2006.06.004.